Journal of Molecular Liquids 385 (2023) 122360

Contents lists available at ScienceDirect

Journal of Molecular Liquids

journal homepage: www.elsevier.com/locate/molliq

Giant permittivity in dimethylamino-terminated ferroelectric nematogens

Martin Cigl [a], Natalia Podoliak [a], Tomáš Landovský [a], Dalibor Repček [a,b], Petr Kužel [a], Vladimíra Novotná [a,*]

[a] Institute of Physics of the Czech Academy of Sciences, Na Slovance 2, Prague, Czech Republic
[b] Faculty of Nuclear Sciences and Physical Engineering, Czech Technical University in Prague, Břehová 7, Prague, Czech Republic

A B S T R A C T

Since the recent discoveries, ferroelectric nematics became of upmost interest due to their outstanding ferroelectric properties. In this work, we prepared a series of polar molecules revealing a ferroelectric nematic phase (N_F) with a very high dielectric constant ($>10^4$). A new motif, which differs from previously reported molecular structures, was optimized to support the N_F phase. For all homologues the N_F phase was observed directly on the cooling from the isotropic phase and ferroelectric behaviour was investigated by dielectric spectroscopy, second harmonic generation, polarization current measurements and by analysis of textures in the polarized light. The presented materials combine ferroelectricity with giant permittivity in a fluid media at room temperatures, so they appear to be extremely attractive. Polarity of molecules with the strong susceptibility to the electric field represent high potential for various applications in energy-efficient memory devices or capacitors.

1. Introduction

In thermotropic liquid crystals (LCs) the molecules can self-assemble and create intermediate phases (mesophases) in a certain temperature range between liquid and crystalline phases [1], combining the fluidity of liquids with the anisotropy characteristic for crystals. Anisotropic properties of LC medium manifest itself as a result of the anisotropic shape of (partially) ordered constituent molecules. A large variety of phases and structures can be observed in LCs, which are susceptible to external field and boundary conditions. Many LC phases reveal a large electro-optical response, which became a background of mass-production technological applications (monitors, sensors, etc.). First, the ferroelectricity in LCs was associated with chirality of the constituent molecules and only a tilted smectic phase formed by chiral rod-like molecules [1] was considered to feature ferroelectricity (FE) and/or antiferroelectricity (AF). With the discovery of bent-core materials [2], it was found that non-chiral mesogens may also form FE and AF phases as the close packing and hindered rotation can lead to the structural chirality. Nevertheless, due to a higher viscosity, smectic phases never reached such broad application range as nematics.

Recent discoveries stimulated renewed intensive progress in the field of nematic liquid crystals. For a conventional nematic phase, the director orientations n and $-n$ are indistinguishable due to the thermal fluctuations, so they form only non-polar phases. However, as far back as in 1918, Max Born [3] predicted a possibility of a ferroelectric fluid, in which all the dipoles point in the same direction. In such a nematic ferroelectric state (N_F), the dipole moments μ should be strong enough such that the dipole–dipole interactions overwhelm the thermal fluctuations. In 2017, a real breakthrough was announced in the development of LCs, as the first two ferroelectric nematics (denoted RM734 and DIO) were reported simultaneously by two research teams [4–6]. Both materials reveal extremely high longitudinal dipole moments (about 10 D), anomalously huge dielectric anisotropy $\Delta\varepsilon$, and a spontaneous polarisation of about 4 μC/cm^2, which is an order of magnitude higher than the previously reported values in other ferroelectric LC phases. Recently, these materials have been intensively studied [7–17]. Mandle at al. [9] synthesised a homologue series relevant to the molecular structure of RM734 and analysed the mesomorphic properties and tendencies leading to the N_F phase. The compounds have been intensively studied by Ljubljana researchers [10–12] and by the Boulder group [13,14]. The existence of ferroelectric domains with a different macroscopic orientation of the dipoles in the absence of electric field was reported [10–14]. Details of polar nature of self-assembly, evolution of topological objects and analysis of their character [12,17,18] are under intensive research progress. Currently, the research is focused on the preparation and characterisation of new compounds with the aim to improve physical properties towards applications. Machine learning procedures were employed to predict ideal conditions for the N_F phase presence, including a dipole moment value, aspect ratio, length of the molecule as well as the dipolar angle [19]. In spite of the fact that these

* Corresponding author.
E-mail address: novotna@fzu.cz (V. Novotná).

https://doi.org/10.1016/j.molliq.2023.122360
Received 6 February 2023; Received in revised form 2 May 2023; Accepted 14 June 2023
Available online 20 June 2023

conditions are rather restrictive, development in the designing of prosperous molecular structures was promoted. In the future, an intensive research concerning polar properties is anticipated for the N_F phase due to its fluidity combined with rather high permittivity. Thin films can be easily deposited or reached by a capillary action, which is promising for device integration and miniaturization in various devices.

At the moment, microscopic organisation of the polar molecules and the mechanism of the phase transition to the ferroelectric nematic phase undergo intensive research and stimulating debates. A theoretical description of the ferroelectric nematic phase has been proposed [20,21], and chiral analogues of highly polar molecules were developed recently [22]. Additionally, a possibility of oligomer synthesis was shown [23] and new phases and effects introduced. In any case, the ferroelectric properties combined with the giant permittivity in a fluid media represent an attractive rapidly developing subject. Since the discovery of N_F phase, the ongoing research is mostly concentrated on the design of new molecular structures. Up to now, the library of N_F materials is strictly limited to a couple of general structures possessing a suitable aspect ratio and a large enough dipole moment, which develops due to the effective electron donating and withdrawing groups within the molecules.

In this contribution, we demonstrate newly designed structural motif (see Fig. 1). In contrast to the previously reported molecular designs [3–5,8–19], which utilise an oxygen-based electron donating group, we synthesised a series possessing a more efficient nitrogen electron donating group in the terminal part of the aromatic system. Such a design yields higher dipole moment along the long molecular axis compared to other published materials. To modify the lateral interactions, which are strong in highly polar systems, we introduced a lateral alkyl chain with varied number of carbon atoms from 1 to 6. Based on these considerations, we synthesised a series of compounds (Fig. 1) which exhibit the N_F phase directly below the isotropic liquid on cooling. By tuning the lateral substitution, we shifted the phase range of N_F down to the room temperature. at which it may eventually relax to a stable glassy state preserving the ferroelectric behaviour.

2. Materials and methods

The synthetic route of the studied mesogens (Fig. 1) is schematically depicted in Scheme 1. Synthesis of materials started from commercial 4-aminosalicylic acid (**1**). Its amino group was protected by acetylation and the carboxylic group was protected by alkylative esterification by methyl iodide, so as neither of the two groups interfere with the alkylation of phenolic hydroxyl. Protected derivative **2** was then alkylated by 1-bromoalkanes to get a series of alkyl homologues **3-n**. In the next steps, the acetyl group was cleaved by acidic hydrolysis under mild conditions and the liberated amino group was alkylated by dimethyl sulphate yielding the key intermediate, acid **4-n**. The lowest alkyl homologue (**4**–**1**) was synthesised directly from acid **1** by alkylation with the excess of dimethyl sulphate. The second part of the molecular core was synthesised from 4-hydroxybenzoic acid (**5**), which was protected by the reaction with 3,4-dihydro-2H-pyrane and reacted with 4-nitrophenol in a *N,N'*-dicyclohexylcarbodiimide-mediated esterification. The protected hydroxyl group was then liberated by the treatment with *p*-toluenesulfonic acid. The final step of the synthesis was esterification of acids **4-n** with phenol **6** mediated by 1-ethyl-3-[3-(dimethylamino) propyl]carbodiimide.

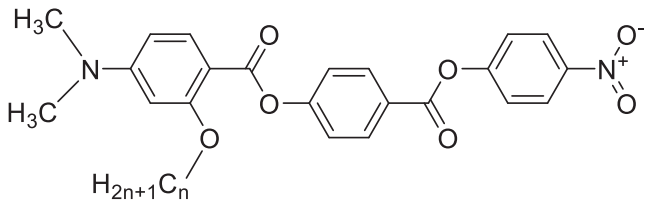

Fig. 1. Chemical formula of compounds **NFn** with n = 1–6.

Differential scanning calorimetry (DSC) measurements were performed to acquire thermal properties. For electro-optical studies, a polarising optical microscope was used, equipped with a heating/cooling stage. Details about the compound characterisation and experimental apparatus are in Supplemental file. A home-made cell for polarization measurements is shown in Fig. S1 and a scheme for the second-harmonic (SHG) measurements is presented in Fig. S2.

3. Results

We studied all newly synthesised homologues by DSC and observed textures and their changes in polarising microscope to assess the phase behaviour. We performed DSC measurements in a broad range of temperatures, *T*. For the first heating process we observed a direct transformation from the crystalline to the isotropic (Iso.) phase. On the subsequent cooling down to −25 °C, the compounds transformed to the liquid crystalline state at a significantly lower temperature, T_c. Under the polarising microscope, we observed characteristic textures for a nematic phase. In specific geometries, the textures revealed the features described to the ferroelectric nematic phase, N_F [12–18]. In the following description, the ferroelectric character of the N_F phase is systematically uncovered.

The results of the DSC data analysis are summarised in Table 1. The samples were heated from the room temperature to the isotropic phase, then cooled down to −25 °C, stabilized for 1 min and heated again up the maximum temperature of the first heating run. For the first heating of the sample, the melting point (m.p.) was established (Table 1). All homologues revealed the ferroelectric nematic phase, N_F, on cooling of the sample below the T_c temperature. Compounds **NF1**, **NF2**, and **NF3** do not show any crystallisation peak during the DSC cooling runs. An exothermic peak was observed on the subsequent heating curves (see example Fig. S3 for **NF3**). For thermal studies of these homologues, the temperature stabilisation or heating of the sample can cause a gradual crystallisation. The homologue **NF4** revealed the shortest temperature range of the N_F phase and it crystallised at 74 °C. For the longest homologues **NF5** and **NF6**, the situation is more complex as these compounds did not show any crystallization peak during cooling-heating runs (for **NF5** see Fig. 2, DSC thermographs for **NF6** is presented in Fig. S4). For **NF5** we repeated the DSC measurements after stabilization of the sample at the room temperature for 18 h and the heating curve is demonstrated in Fig. 2 as a black line. One can see two endothermic peaks during the heating process, smaller peak at the T_C temperature and another peak at the melting point. It corresponds to our observation under a polarizing microscope, we pursued the N_F phase persistence in several heating–cooling cycles and/or at a stabilized temperature. The crystallization started after several hours gradually. The glassy transition was clearly distinguishable for all compounds and the glassy temperature, T_g, was determined from the onset calculated at a half heat capacity, c_p, see Table 1. The glassy transition with a typical shape is marked by an arrow at the heating thermographs for **NF5** in Fig. 2. Glassy properties and formation of fibres from the melted compound **NF5** is demonstrated in Supplemental file (Fig. S5).

In the polarising microscope, we observed various textural features in different commercial or home-made cells. There are two basic geometries for rod-shaped liquid crystalline molecules: in HG cells, the molecules are oriented along the cell surface, and in the HT cell, a homeotropic anchoring ensured molecular orientation perpendicular to this direction. In the HG cell, the alignment is provided by rubbed polyimide layers with a small pretilt to arrange defect-free textures. The pretilt results in nonzero polar surface energy as was pointed out by Chen et al. [14]. Two kinds of HG cells were available, with parallel (HG-P) or antiparallel (HG-A) rubbing directions on opposite glass surfaces.

Let us start with HG-A cells and compare the results for various cell thicknesses. In this geometry, we observed two kinds of domains. The texture in 5 μm HG-A cell for the studied homologue **NF6** is shown in

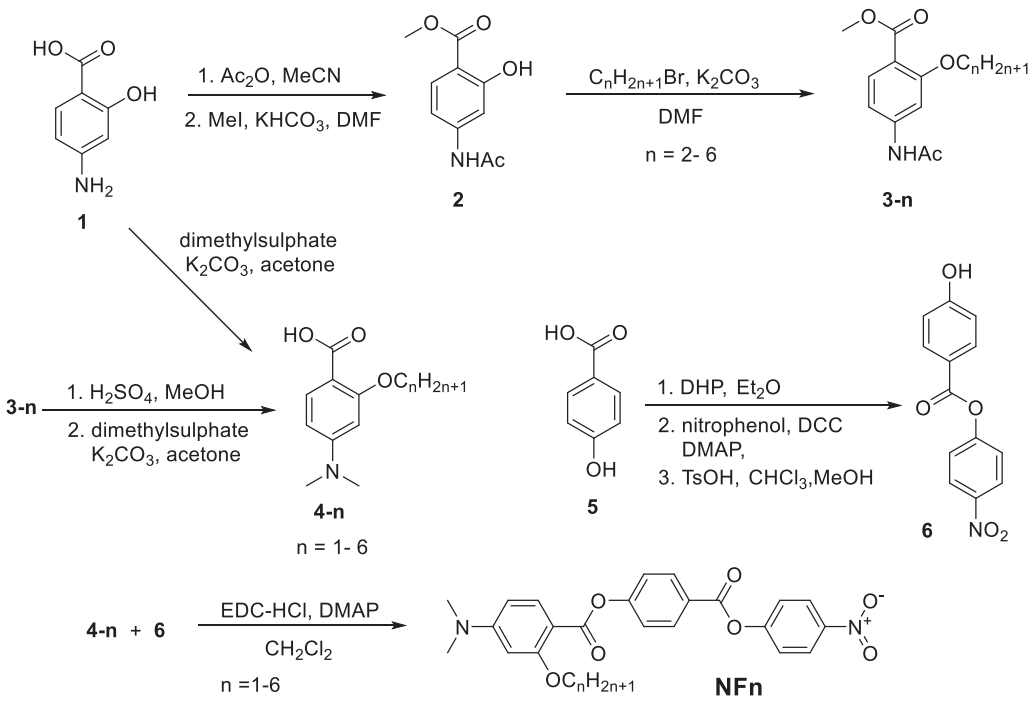

Scheme 1. Synthesis of the studied polar nematogens denoted **NFn** with *n* varying from 1 to 6.

Table 1
Calorimetric data taken from DSC measurements: melting point, m.p., was detected at the first heating run, the N_F-Iso phase transition temperature, T_c, at the second cooling and the glassy transition temperature, T_g, was established from the second heating run. All temperatures are presented in °C, and the enthalpy changes, ΔH, are in square brackets at the corresponding temperatures.

	m.p. (°C) ΔH (J/g)	T_c (°C) ΔH (J/g)	T_g (°C) ΔH (J/g)
NF1	188 [+98.6]	170 [-2.73]	24 [+0.47]
NF2	150 [+71.3	136 [-7.59]	30 [+0.42]
NF3	156 [+73.8]	116 [-7.13]	15 [+0.27]
NF4	144 [+80.2]	96 [-6.11]	–
NF5	120 [+55.1]	82 [-4.86]	−9 [+0.44]
NF6	104 [+51.4]	65 [-3.33]	4 [+0.28]

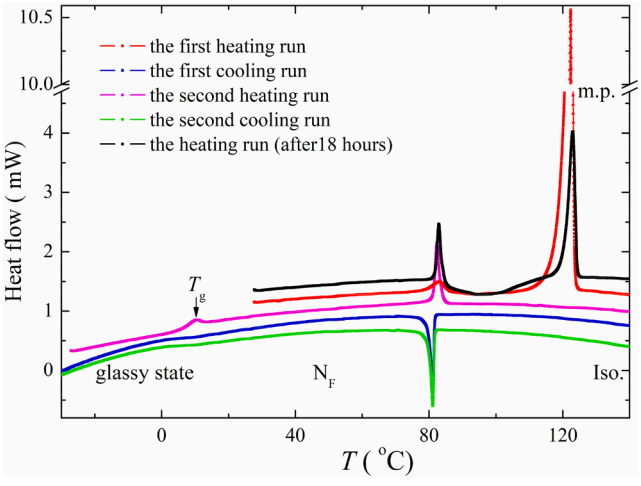

Fig. 2. DSC thermograph detected for **NF5** during the first and second heating and cooling runs. The slopes and a relative shift in the heat flow were adjusted for convenience.

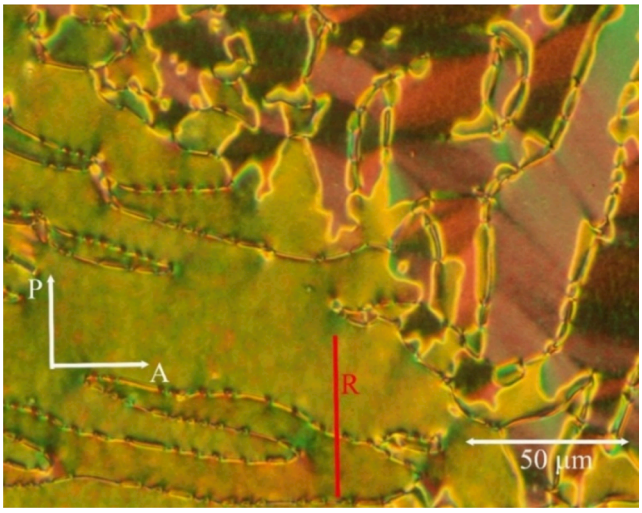

Fig. 3. Microphotograph of **NF6** homologue in 5 µm HG-A cell. The red arrow (R) marks the rubbing direction, the white arrows show the polariser (P) / analyser (A) directions.

Fig. 3. The dominating type of domains are twisted domains, which were described for the N_F phase in literature [12]. The twisted domains are recognisable when slightly uncrossing the analyser from the crossed position. Another type of domains can be observed in less extensive areas of the HG-A samples. In the upper right part of Fig. 3, we found "red-colour" domains with characteristic borderline approximately parallel to the rubbing direction. The red colour was typical for these domains in 5 µm HG-A cell, see Fig. S6 in Supplemental for other homologues. Extinction positions in these domains are not easy to be established and the colour of these domains changes when rotating the sample with respect to the polariser position. We did not find twisted domains in HG-P cells with parallel alignment. In this geometry, we observed homogeneously aligned area and other type of domains, as is demonstrated for **NF6** in Fig. S7 in Supplemental file.

We concentrate on twisted domains, which are very frequent in the HG-A geometry. We found that for very thin HG-A sample, the twisted domains were extended for a large area by quick cooling from the isotropic phase (with a rate > 20 K/min). Rather big domain areas separated by a zig-zag borderline are demonstrated in Fig. 4(a) for **NF6** in 1.6 μm HG-A cell. One can see that the borderline between the twisted domains is oriented approximately perpendicularly to the rubbing direction. When we turn the analyser from the crossed position by an angle of ~ 20°clockwise or anticlockwise, we can distinguish two kinds of domains (see Fig. 4(c) and Fig. 4(d)). The sense of twist is opposite for two neighbouring domains and they are separated by 2π disclination line. Schematic picture of molecular twist between surfaces with antiparallel alignment is shown in Fig. 4(b). In the paper by Sebastian [12], similar domains were observed for another type of ferroelectric nematogen and designated "sierra-domains". In our particular case, these twisted domains reveal sharper contour and can be renamed as "shark-domains". For the homologue **NF5**, the twisted domains are shown in Fig. S8 in Supplemental.

An application of an electric field in HG geometry led to a rather complex effect, the colour of twisted domains slightly changes and a detail analysis is rather problematic. As we preferred to apply the field along the molecular director, we utilized the HT cells. In this geometry, we can observe a rearrangement of molecules under the applied field. In Fig. 5, we demonstrate the HT texture for homologue **NF6** with and without applied electric field of about 5 V/μm. In the upper part of Fig. 5, an area without electrode is observed. It is necessary to point out that under the field (Fig. 5(b)), the molecules reorient along this direction and the texture under the electrode area becomes black. After switching the electric field off, the HT texture turns back to a coloured character, similar to the virgin texture (Fig. 5(a)), within several seconds.

We investigated the switching properties of the studied compounds in HT geometry. Due to electrostatic interactions, the results are influenced both by the cell geometry and by the character of the aligning layer. For n = 1–4, the homologues **NFn** reveal strong vitrification and an increase in viscosity when approaching the glass transition temperature T_g. This temperature is relatively high and the samples feature a higher conductivity, which limited our studies for these homologues. On the contrary, homologues **NF5** and **NF6** could be subjected to the applied field for a longer time and even after several hours they still revealed an electro-optical response. Nevertheless, to avoid a breakdown, we tried to apply a small measuring field, only up to 5 V/μm.

To analyse the effect of the applied electric field in different cell geometries, we prepared a home-made gap-cell with in-plane electrodes, which is schematically demonstrated in Fig. S2 in Supplemental file. Two glass slides were separated by copper ribbons 35 μm thick, with a gap distance of about 1 mm. In this cell, the domains disappeared under the applied electric field as all the molecules were aligned along the applied electric field (see Fig. S9). After the switching-off of the external electric field, the domain structure was partially reconstructed in several seconds. Unfortunately, the thickness of 35 μm was rather large to reach homogeneous alignment through the whole cell thickness and analyse domain behaviour. Additionally, we are aware that the applied electric field was not homogeneous within the cell thickness. Technological tasks of the cell preparation and detailed analysis of the defects in electric field are still under work.

The polarisation, *P*, was studied in an a.c. filed and its values calculated by the time-integration of a switching current profile. For homologue **NF5**, the temperature dependence of the polarisation is presented in Fig. 6(a). In Fig. 6(b), the switching current is plotted versus the applied electric field at a frequency 10 Hz and at temperature 52 °C. For both homologues **NF5** and **NF6,** we detected a continuous increase in polarisation values on cooling process in the N_F phase. A coexistence of the Iso and N_F phases was checked under the polarising microscope and we observed it only in a narrow temperature interval of about 2 °C. The decrease in polarisation values shown in Fig. 6(a) is connected with an increase in switching time. Such a slowing-down of molecular dynamics is connected with an increase in the sample viscosity. The polarisation curves were measured repeatedly and the results were reproducible.

We measured the dielectric spectra of all compounds in a temperature range from the isotropic liquid to room temperatures in order to study the molecular dynamics. The applied measuring field was smaller than 0.02 V/μm. Higher probing fields influenced the dielectric

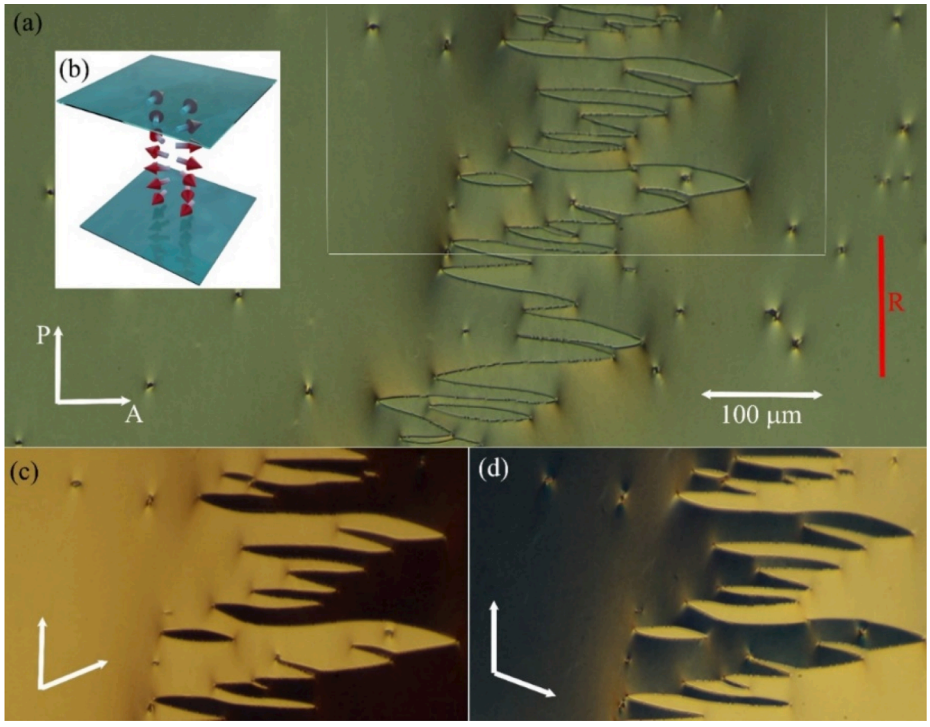

Fig. 4. Textures of **NF6** in 1.6 μm HG-A cell under a polarizing microscope (a) between crossed polarisers, the red arrow marks the rubbing direction, R, the orientation of the analyser (A) and the polariser (P) is schematically shown by white arrows. In the figure (b) there is a schematic arrangement of molecules in neighbouring twisted domains between glass surfaces with antiparallel rubbing. The part of the figure (a) marked by white lines is shown in (c) and (d) when A is rotated by an angle of about 20°anticlockwise or clockwise from the crossed position.

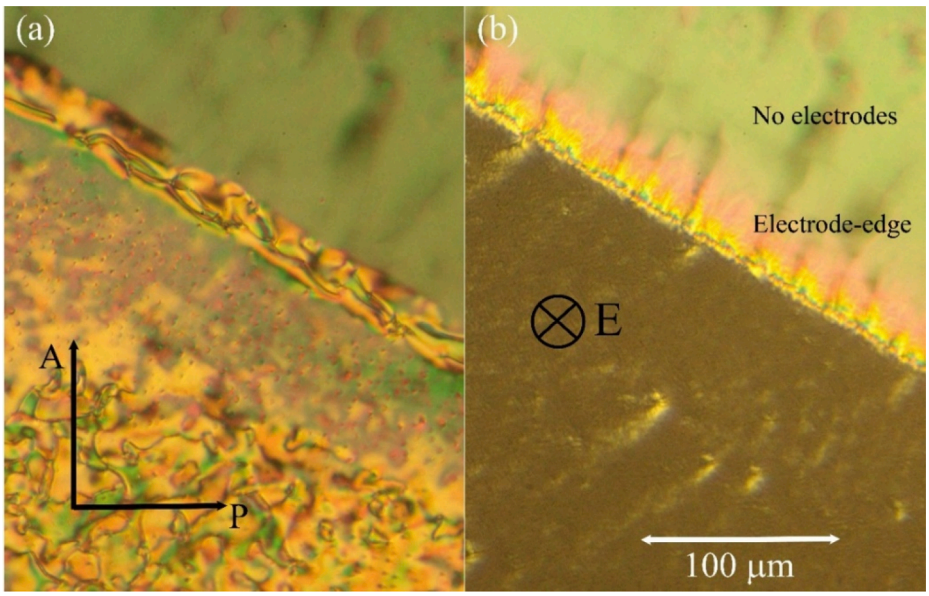

Fig. 5. Texture of **NF6** in 5 μm thick HT cell, (a) without electric field and (b) under applied electric field of about 5 V/μm perpendicular to the cell. The orientation of polarisers and of the applied electric field are marked by black symbols for illustration. Upper part of the figure shows an area without electrodes.

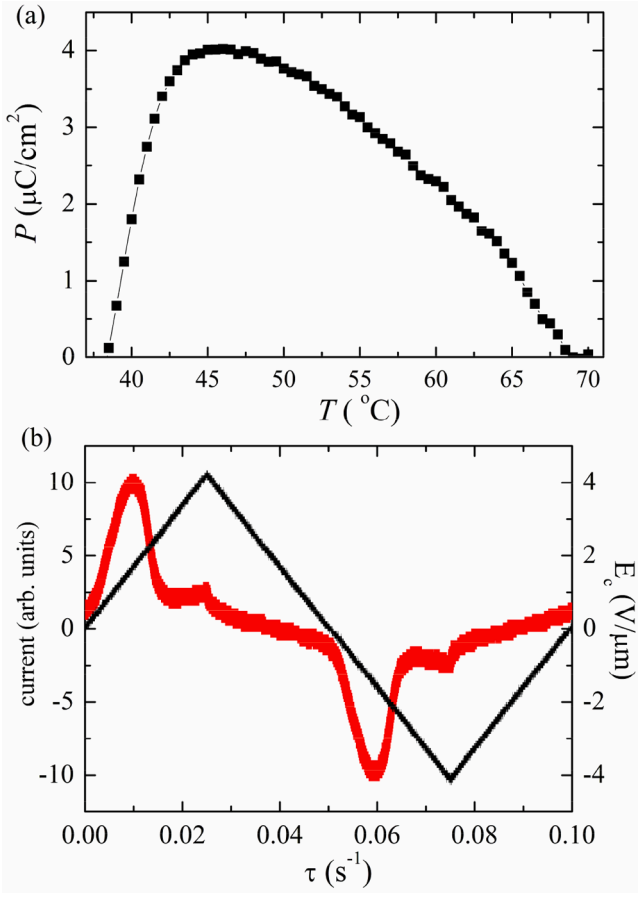

Fig. 6. (a) The temperature dependence of the polarisation of **NF5**, which was calculated from the polarisation current. (b) The current profile at a temperature T = 52 °C is demonstrated with a triangular profile of the applied electric field at a frequency 10 Hz.

measurements as the studied compounds are really sensitive to it. In the ferroelectric N_F phase, we found one distinct quite strong relaxation mode appearing at the Iso-N_F phase transition on cooling and remaining visible down to the room temperature. On the other hand, when the sample is in the crystalline state, this mode is not present and the permittivity is low (<10). We demonstrate three-dimensional plots of the real, ε', and imaginary, ε'', parts of permittivity versus frequency and temperature, *T*, for compound **NF5** in Fig. 7. For homologues **NF2**, **NF3** and **NF6,** the 3D-plots of permittivity are shown in Supplemental file, Figs. S10-S12. All the presented dielectric data were obtained in 12 μm thick cells with gold electrodes and no surfactant layers.

We encountered a disturbing effect of surfactant, similarly as it was mentioned in previous works dealing with dielectric spectroscopy of the N_F phase [16]. For such a type of polar phase, it was reported that the polymer layers effectively influence the permittivity measurements. Due to a non-conductive character of polymer layers on the cell surfaces, there is a barrier which causes a spatial variation of the charge and influences the measured effective permittivity values. We fitted the dielectric data to the Cole-Cole formula (see Supplemental file for the details) to obtain information about the dielectric strength, Δε, and the relaxation frequency, f_r. For all homologues we detected extremely big values of Δε, higher than 15×10^3. The dielectric strength is growing during the cooling process below the phase transition temperature T_c and after that it starts to very moderately decrease. In Supplemental file in Fig. S13, we compared Δε(T) for all homologues and concluded that the values do not differ significantly. Probably, the role of the side-chain length (*n* number) is important mostly for the phase transition temperatures, not for the polar properties.

In contrast, the relaxation frequency decreases within the whole temperature range of the N_F phase on cooling. Such behaviour is documented in Fig. 8 for homologue **NF5**, which followed Arrhenius behaviour ideally and the activation energy, E_A, was calculated to be 94 kJ/mol**.** For other compounds, the linearity of f_r in logarithmic scale (versus 1/T in absolute temperature scale) was confirmed only far from the Iso-N_F phase transition. In Fig. S13, the dielectric strength, Δε, and the relaxation frequency, f_r, is shown for **NF6**. As the cell with gold electrodes is rather thick (12 μm), we can expect non-homogeneous molecular arrangement within the cell thickness, which should be taken into consideration to explain the deviation from Arrhenius law.

Strong polar character of the N_F phase was proven by SHG measurements. The SHG experiments were carried out in a transmission

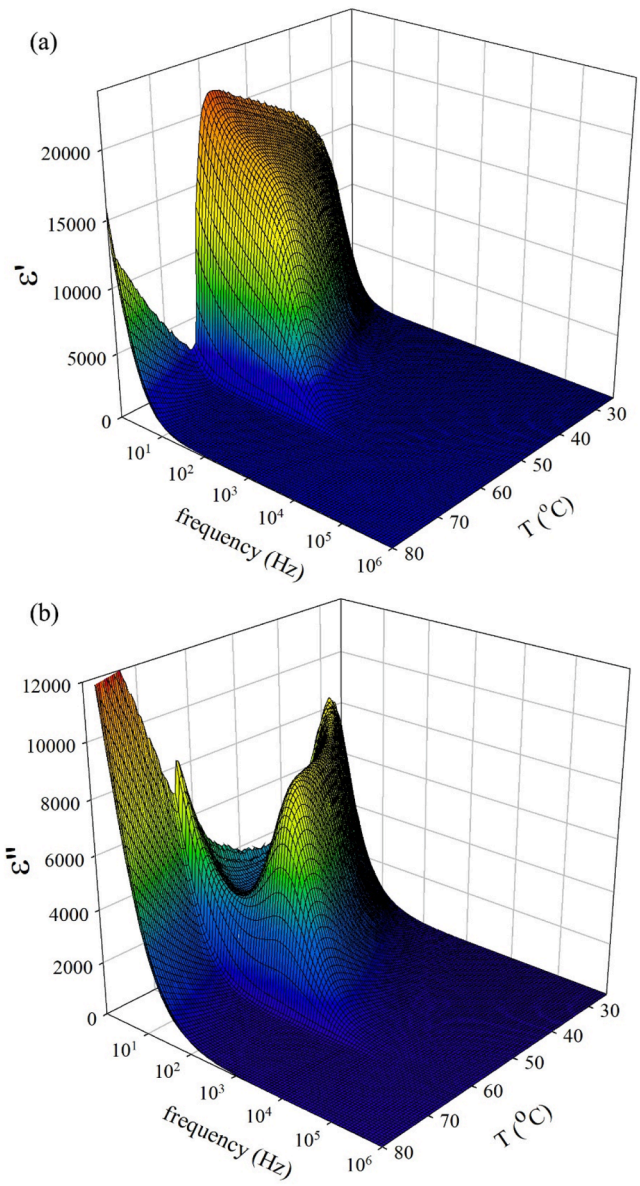

Fig. 7. 3D-plot of (a) the real, ε', and (b) the imaginary, ε'', part of the permittivity versus frequency and temperature, *T*, for compound **NF6**. Dielectric measurements were performed in 12 μm cell with gold electrodes and no surfactant layer.

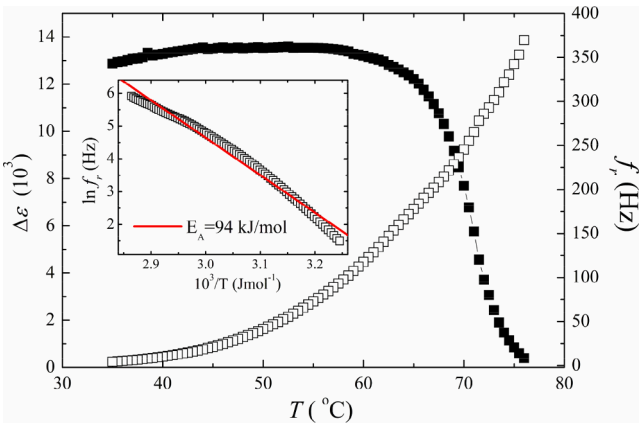

Fig. 8. Temperature dependences of the dielectric strength, Δε, and the relaxation frequency, f_r, for **NF5** in 12 μm home-made cell without surfactant layer. In the inset f_r is presented in the logarithmic scale versus reciprocal temperature in Kelvins, 1/T. The activation energy E_A was established from the slope.

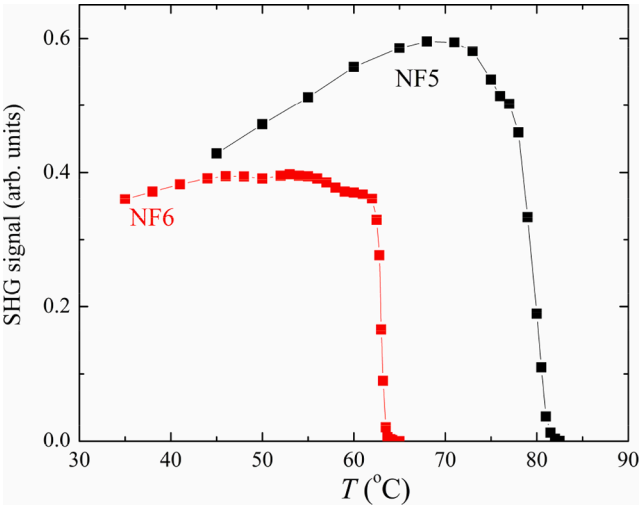

Fig. 9. SHG signals for **NF5** and **NF6** in HG cells.

configuration according to the scheme described in Supplemental file. We utilised HG cells and SHG measurement results are presented for compounds **NF5** and **NF6** in Fig. 9. On cooling the sample from the isotropic phase, the SHG signal abruptly grows from zero value at the transition temperature to N_F phase. With ongoing temperature decrease, the SHG intensity slows down its increase, reaches the maximum and slowly starts to decrease. All of this happens within the N_F phase, where we would expect a gradual increase in the SHG signal upon cooling. Moreover, even for the weakest applied intensity of the fundamental laser beam, a small drop in SHG intensity was detected in subsequent measuring runs at the same temperature. From this it follows that the decrease in the SHG signal upon cooling may be explained by partial decomposition of our samples caused by rather strong intensity of the pulse laser beam.

X-ray scattering experiments confirmed nematic assembling in the observed mesophase. Nematic phase is characterised by the long-range orientational order and only broad diffuse peaks of low intensity can be detected. For homologue **NF5**, the signal at small scattering angles is rather wide and can be fitted with two signals, with maxima corresponding to 18.8 Å and 10.5 Å at T = 75 °C, 22.5 Å and 10.4 Å at T = 30 °C. As the length of molecules, *l*, can be approximately established as $l \sim 20.9$ Å, the peak at the small scattering angle matches perfectly to the long dimension of the molecules. The peak at a wide-angle region has also a very broad profile with the maximum corresponding to 4.4 Å for all measuring temperatures, and it corresponds to an average distance between the molecules.

4. Conclusions

We proposed a new structural modification of highly polar molecules self-assembling and forming the ferroelectric nematic phase N_F. All the prepared compounds exhibit a direct phase transition to the ferroelectric nematic phase on cooling from the isotropic phase. In the presented homologue series, a prolongation of a side-chain resulted in the N_F phase persistence down to the room temperatures and stability for at least several hours. Ferroelectric character of the nematic phase was proven by several experimental techniques. Characteristic textural features for the ferroelectric nematics were observed in several sample geometries. The ferroelectric switching process was detected and the polarisation was calculated from the measured polarisation current. The values of

polarisation were found to increase continuously on cooling from the isotropic phase, reaching up to 4 μC/cm^2 for the homologues **NF5** and **NF6**. For shorter homologues, the application of an electric field can initiate a crystallization process and temperature measurements were not accomplished. Quick attempts showed that the polarization values of all homologues are similar and probably do not significantly differ. Nevertheless, the higher homologues **NF5** and **NF6** show a better thermal stability, the samples can be heated/cooled repeatedly and the N_F phase persists for several hours, even if the field was applied.

For all the studied homologues, the dielectric studies show a strong polar mode characteristic for the N_F phase, disappearing in the isotropic or crystalline phases. We compared the dielectric strength, $\Delta\varepsilon$, of this mode and concluded that it does not differ in dependence on the side-chain length described by n number (Fig. S14 in Supplemental). In average $\Delta\varepsilon$ reaches 16×10^3, which exceeds values reported for the LC compounds with the N_F phase up to now. The dipole moment of the molecules was calculated and established to be about 14 D, which is larger than the value reported for DIO or RM734. Nevertheless, to properly characterize the spatial distribution of charge and/or evaluation of the role of the electrodes is very complicated in a confined geometry of the cell. Many questions are still open, as spatially inhomogeneous charges exist in a real sample and complicate the description. A detailed analysis of the origin and character of molecular alignment in different geometries of the cell is under progress.

The discovery of the ferroelectricity in nematics opened new opportunities in the liquid crystal research and generally in the field of condensed matter. The N_F phase represents a highly polar structure responsive to very small applied fields and it features a variety of new effects induced by the confining surfaces. Our particular room-temperature-stable soft phase exhibits a huge dielectric constant and can be important in future for the development of memory devices, capacitors and actuators. New systems based on this type of highly-polar nematogen will be extremely promising if ferroelectricity is combined with other functionalities [24]. In future, we anticipate the preparation of structurally innovative multifunctional nanostructured systems, attractive from many aspects, which would open new lines in Soft Matter research.

Declaration of Competing Interest

The authors declare that they have no known competing financial interests or personal relationships that could have appeared to influence the work reported in this paper.

Data availability

Data will be made available on request.

Acknowledgments

The study was funded from the European Union's Horizon 2020 research and innovation programme by the project MAGNELIQ under grant agreement No 899285. The results reflect only the authors' view and the Commission is not responsible for any use that may be made of the information it contains. V.N., N.P., and M.C. acknowledge project 22-16499S from the Czech Science Foundation. D.R. thanks to Grant Agency of the Czech Technical University in Prague (Project No. SGS22/182/OHK4/3T/14). V.N. is grateful to Damian Pociecha and Ewa Gorecka from Warsaw University for their help with x-ray measurements.

Appendix A. Supplementary material

Supplementary data to this article can be found online at https://doi.org/10.1016/j.molliq.2023.122360.

References

[1] Handbook of Liquid Crystals, 2nd Edition, ed. In: J. W. Goodby, P. J. Collings, T. Kato, C. Tschierske, H. Gleeson, P. Raynes, Wiley-VCH, 2014.
[2] H. Takezoe, Y. Takanishi, Bent-core liquid crystals: Their mysterious and attractive world, Jpn. J. Appl. Phys. 45 (2A) (2006) 597–625.
[3] M. Born, Über anisotrope Flüssigkeiten. Versuch einer Theorie der flüssigen Kristalle und des elektrischen Kerr-Effekts in Flüssigkeiten, Annals of Physics 55 (1918) 221.
[4] R.J. Mandle, S.J. Cowling, J.W. Goodby, A nematic to nematic transformation exhibited by a rod-like liquid crystal, PCCP 19 (2017) 11429–11435.
[5] H. Nishikawa, K. Shiroshita, H. Higuchi, Y. Okumura, Y. Haseba, S. Yamamoto, K. Sago, H. Kikuchi, A fluid liquid-crystal material with highly polar order, Adv. Mater. 29 (2017) 1702354.
[6] R.J. Mandle, S.J. Cowling, J.W. Goodby, Rational design of rod-like liquid crystals exhibiting two nematic phases, Chem. Eur. J. 23 (2017) 14554–14562.
[7] O.D. Lavrentovich, Ferroelectric nematic liquid crystal, a century in waiting, PNAS 117 (26) (2020) 14629–14631.
[8] A. Mertelj, L. Cmok, N. Sebastian, R.J. Mandle, R.R. Parker, A.C. Whitwood, J. W. Goodby, M. Čopič, Splay nematic phase. *Physical Review X* 8 (2018), 041025.
[9] R.J. Mandle, S.J. Cowling, J.W. Goodby, Structural variants of RM734 in the design of splay nematic materials, Liq. Cryst. 48 (12) (2021) 1780–1790.
[10] N. Sebastian, L. Cmok, R.J. Mandle, M. Rosario de la Fuente, I. Drevenšek Olenik, M. Čopič, A. Mertelj, Ferroelectric-ferroelastic phase transition in a nematic liquid crystal, Phys. Rev. Lett. 124 (2020), 037801.
[11] N. Sebastian, R.J. Mandle, A. Petelin, A. Eremin, A. Mertelj, Electrooptics of mm-scale polar domains in the ferroelectric nematic phase, Liq. Cryst. 48 (14) (2021) 2055–2071.
[12] N. Sebastián, M. Copic, A. Mertelj, Ferroelectric nematic liquid-crystalline phases, Phys. Rev. E 106, 106 (2022), 021001.
[13] Polar domains and striking electro-optics, X. Chen, E. Korblova, D. Dong, X. Wei, R. Shao, L. Radzihovsky, M.A. Glaser, J.E. Maclennan, D. Bedrov, D.M. Walba, N.A. Clark., First-principles experimental demonstration of ferroelectricity in a thermotropic nematic liquid crystal, PNAS 117 (2020) 14021–14031.
[14] X. Chen, E. Korblova, M.A. Glaser, J.E. Maclennan, D.M. Walba, N.A. Clark, Polar in-plane surface orientation of a ferroelectric nematic liquid crystal: Polar monodomains and twisted state electro-optics, PNAS 118 (22) (2021) 2104092118.
[15] A. Manabe, M. Bremer, M. Kraska, Ferroelectric nematic phase at and below room temperature, Liq. Cryst. 48 (2021) 1079–1086.
[16] S. Brown, E. Cruickshank, J.M.D. Storey, C.T. Imrie, D. Pociecha, M. Majewska, A. Makal, E. Gorecka, Multiple polar and non-polar nematic phases, ChemPhysChem 22 (2021) 2506–2510.
[17] F. Caimi, G. Nava, R. Barboza, N.A. Clark, E. Korblova, D.M. Walba, T. Bellini, L. Lucchetti, Surface alignment of ferroelectric nematic liquid crystals, Soft Matter 17 (2021) 8130–8139.
[18] P. Rudquist, Revealing the polar nature of a ferroelectric nematic by means of circular alignment, Sci. Reports 11 (2021) 24411.
[19] J.X. Li, H. Nishikawa, J. Kougo, J. Zhou, S. Dai, W. Tang, X. Zhao, Y. Hisai, M. Huang, S. Aya, Development of ferroelectric nematic fluids with giant dielectricity and nonlinear optical properties. *Science*, Advances 7 (2021) eabf5047.
[20] N.V. Madhusudana, Simple molecular model for ferroelectric nematic liquid crystals exhibited by small rodlike mesogens, Phys. Rev. E 104 (2021), 014704.
[21] E.I. Kats, Stability of the uniform ferroelectric nematic phase, Phys. Rev. E 103 (2021), 012704.
[22] X. Zhao, J. Zhou, J. Li, J. Kougo, Z. Wan, M. Huang, S. Aya. Spontaneous helielectric nematic liquid crystals: Electric analog to helimagnets. *PNAS*, 118 (42) (2021) e2111101118.
[23] J. Li, R. Xia, H. Xu, J. Yang, X. Zhang, J. Kougo, H. Lei, S. Dai, H. Huang, G. Zhang, F. Cen, Y. Jiang, S. Aya, M. Huang, How far can we push the rigid oligomers/polymers toward ferroelectric nematic liquid crystals? J. Am. Chem. Soc. 143 (2021) 17857–17861.
[24] H. Nishikawa, K. Sano, F. Araoka, Anisotropic fluid with phototunable dielectric permittivity, Nature Commun. 13 (2022) 1142.